DESIGN AND GLOBAL OPTIMIZATION OF HIGH-EFFICIENCY THERMOPHOTOVOLTAIC SYSTEMS

THERMO PHOTOVOLTAIC GENERATION OF ELECTRICITY
TPV-9 CONFERENCE 2010

Peter Bermel,* Walker Chan, Yi Xiang Yeng, John D. Joannopoulos, Marin Soljacic, and Ivan Celanovic
Institute for Soldier Nanotechnologies, Massachusetts Institute of Technology,
77 Massachusetts Ave., Cambridge, MA 02139, USA
(Dated: September 3, 2010)

Despite their great promise, small experimental thermophotovoltaic (TPV) systems generally exhibit modest power conversion efficiencies (2.4% or less), mostly due to heat losses such as thermal emission of undesirable mid-wavelength infrared radiation. Photonic crystals (PhC) have the potential to strongly suppress such losses. However, PhC-based designs present a set of non-convex optimization problems requiring efficient objective function evaluation and global optimization algorithms. Both are applied to two example systems: improved micro-TPV generators and solar thermal TPV systems. Micro-TPV reactors experience up to an 11-fold increase in their efficiency and power output; solar thermal TPV systems see an even greater 24-fold increase in their efficiency (exceeding the Shockley-Quiesser limit for a single-junction photovoltaic cell).

1 INTRODUCTION

Thermophotovoltaic (TPV) systems convert heat into electricity by thermally radiating heat onto a low-bandgap photovoltaic (PV) diode, known as a TPV diode [1–5]. In principle, the efficiency of this process can approach the Carnot limit [6]. However, in practice, efficiencies observed in experimentally tested systems are often dramatically lower, ranging from 0.8% or less [7, 8] up to 2.4% [9, 10]. While losses occur at multiple stages in these systems, one of the foremost sources of loss is emission of thermal photons with energy below the TPV bandgap. This reduces the fraction of emitted power containing useful photons, and also tends to heat up the temperature-sensitive TPV diode.

Photonic crystals (PhCs) offer an unprecedented ability to control and mold the flow of light [11]. The most important property of a PhC is its full photonic bandgap (PBG) – a range of frequencies over which light of all incident angles and polarizations is completely reflected. In the context of TPV, PhCs can play an important role in reducing problems associated with below-bandgap photons in several ways. First, they can introduce a PBG in order to suppress emission at critical near-IR wavelengths [12, 13]. This concept was advocated in Refs. 4 and 14. Second, they can enhance emissivity for photon energies above the TPV electronic bandgap, via Q-matching – an approach implicitly utilized in Refs. [15] and [16], and discussed theoretically in Refs. 8 and 17. Finally, they can reflect low-energy photons back to the source – an approach referred to as "photon recycling" [3, 5].

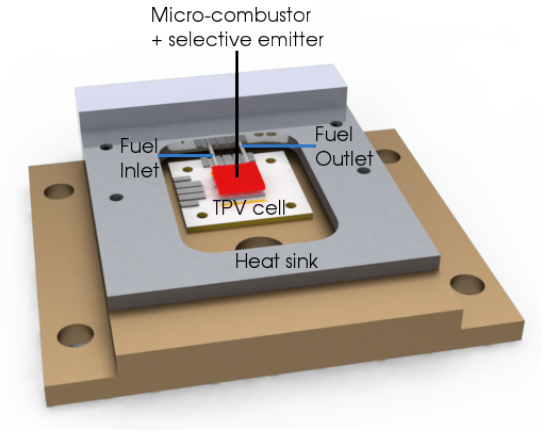

FIG. 1: Illustration of a μTPV system. An inlet brings fuel to the micro-combustor with a selective emitter on its surface. It radiates onto TPV cells above and below, which generates an output current routed through a maximum power-point tracker (not shown).

In this paper, all three unique properties of PhCs are applied to two particular problems: a portable power generation system known as a μTPV generator, and a utility-scale renewable power generation system for converting sunlight into electricity. The μTPV portable power generator illustrated in Fig. 1 boasts a very small form factor, high power density, and flexibility in terms of fuel source. The solar TPV system illustrated in Fig. 2 offers greater generation capacity and higher efficiencies in exchange for a larger footprint and higher capital cost.

*Electronic address: bermel@mit.edu

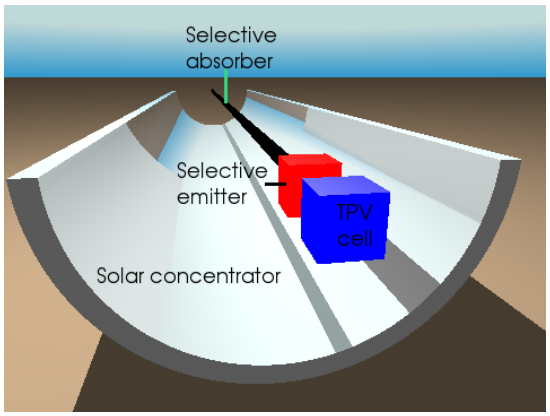

FIG. 2: Illustration of a solar TPV system. Sunlight is collected in a solar concentrator and focused on a selective solar absorber in the middle. It is thermally coupled to a selective emitter, which radiates onto a TPV diode in order to produce electricity.

2 NUMERICAL MODEL

The differential direct view factor dF, measuring the probability of a photon emitted by a blackbody emitter of infinitesimal area dA_1 directly reaching a target area dA_2 at a separation d, is as follows:

$$dF_0 = \frac{\cos\theta_1 \cos\theta_2}{\pi d^2} dA_2, \tag{1}$$

where θ_1 and θ_2 are the angles between the line connecting the two areas and the normal vectors for dA_1 and dA_2, respectively.

The emitted power per unit area $\Phi(\lambda)$ for a blackbody emitter can thus be calculated by integrating over a hemisphere of radius r surrounding the area dA_1:

$$\Phi(\lambda) = \int r^2 I_{\mathrm{BB}}(\lambda) dF_0 = \frac{2\pi hc^2}{\lambda^5 \left[\exp\left(hc/\lambda kT\right) - 1\right]}, \tag{2}$$

where k is Boltzmann's constant, $h = 2\pi\hbar$ is Planck's constant, and T is the temperature of the emitter, which reproduces the well-known result for angle-integrated emission of a blackbody. The total emitted power is then given simply by $P_{\mathrm{em}}(\lambda) = \int dA_1 \Phi(\lambda)$. Following along similar lines, it can be calculated that an emitter with angularly-dependent emissivity $\epsilon(\lambda, \theta)$ will emit power per unit area:

$$\Phi(\lambda) = \frac{2\pi hc^2}{\lambda^5 \left[\exp\left(hc/\lambda kT\right) - 1\right]} \int_0^{\pi/2} d\theta \left[\epsilon(\lambda, \theta) \sin 2\theta\right]. \tag{3}$$

Note that the angle-dependent emissivity can have both diffuse and specular components. This can be captured by defining $\epsilon(\lambda, \theta) = D\epsilon_D(\lambda) + (1 - D)\epsilon_S(\lambda, \theta)$, where D is the diffuse emission fraction (which must fall between 0 and 1).

However, note that some of this emitted power will be reflected back by the receiver. This amount can be calculated as follows. First, following Ref. 18, we can define a differential view factor dF_n for n reflections as follows:

$$dF_n = \frac{\cos\theta'_1 \cos\theta'_{2,n}}{\pi d'^2_n} dA'_n \tag{4}$$

where S_n is a virtual surface constructed via n additional reflections with differential surface area dA'_n, located at a distance d'_n from the initial emitter dA_1. All of the even values of n represent indirect reflection to the opposite surface; odd values represent reflection of the surface back to itself.

The differential power reabsorbed by the emitter will thus be:

$$dP^n_{\mathrm{re}} = \frac{I_{\mathrm{BB}}(\lambda) R_2^{n+1} R_1^n (1 - R_1) \epsilon(\lambda, \theta'_n) \cos^2\theta'_n}{\pi d'^2_n} dA'_n dA_1 \tag{5}$$

Integrating Eq. (5) and summing over odd values of n yields the total reabsorbed power P_{re}.

In order to calculate the total number of photons reaching the opposite surface, the n^{th} contribution to the differential short-circuit current can be written as follows:

$$dI^n_{\mathrm{sc}} = \frac{2qc \cdot \mathrm{EQE}(\lambda) \left(R_1 R_2\right)^{n-1} \epsilon(\lambda, \theta'_n) \cos^2\theta'_n}{d'^2_n \lambda^4 \left[\exp\left(hc/\lambda kT\right) - 1\right]} dA'_n dA_1 \tag{6}$$

where q is the elementary charge of a proton, c is the speed of light, and $\mathrm{EQE}(\lambda)$ is the external quantum efficiency of the TPV diode. The total short-circuit current I_{sc} comes from integrating Eq. (6) and summing over even values of n.

The total current I as a function of applied voltage V is given by $I(V) = I_{\mathrm{sc}} - I_D \left[\exp\left(qV/mkT_{\mathrm{d}}\right) - 1\right]$, where I_D is the total dark current, given by:

$$I_D = \frac{q(n^2 + 1) E_{\mathrm{g}}^2 kT_{\mathrm{d}} A_2}{4\pi^2 \hbar^3 c^2} e^{-E_{\mathrm{g}}/mkT_{\mathrm{d}}} + I_{\mathrm{nr}}, \tag{7}$$

where E_{g} is the bandgap of the TPV device, m is the device ideality factor [19], T_{d} is the device temperature, n is the refractive index of the TPV semiconductor region, I_{nr} is the dark current induced by nonradiative recombination, and V is the applied voltage. The output power is obtained by maximizing the electrical output power (per unit area) $P = IV$ (i.e., by setting $d(IV)/dV = 0$ and back-substituting V). The efficiency η is obtained by dividing P by the integrated net radiative thermal emission $P_{\mathrm{em}} - P_{\mathrm{re}}$.

In order to rapidly compute the emissivity as a function of angle, we employ CAMFR and RODIS, a pair of python-based libraries for computing transmission and reflection for layered structures in any number of spatial dimensions, developed at

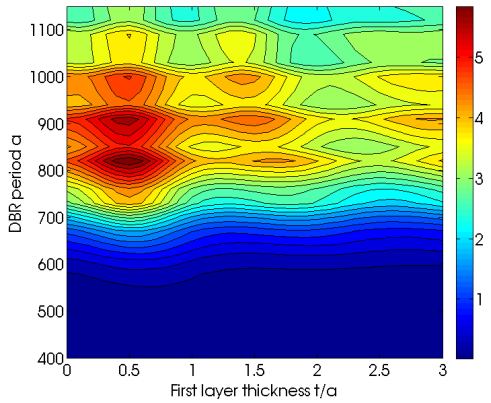

FIG. 3: Contour plot of figure of merit for a 1D PhC selective emitter, as a function of the period a and relative first layer thickness t/a. Note many local optima are observed, particularly in the vicinity of half-integer values of t/a.

the University of Ghent [20, 21]. Previous work has confirmed a close match between their results and time-domain approaches, such as MEEP, which are generally considered to be highly accurate [8, 22].

The temperature of our system for a given thermal input power is determined by making an initial guess for the temperature of the system, followed by a calculation of the output power at such a temperature, then employing the Newton-Raphson method to iteratively converge to the actual equilibrium temperature. Typically, convergence to within 0.1% can be achieved in 5 iterations or less.

In order to determine the optimal parameters for each particular design considered in this paper, we start with the fact that our optimization problem is highly non-convex, marked by a large number of local optima – see, e.g., Refs. 8 and 23. This is demonstrated in the case of μTPV in Fig. 3, where a large number of localized peaks can potentially serve as traps for a local search algorithm. In order to avoid this problem, we employ a global search algorithm instead, as described in Refs. 8 and 23.

3 RESULTS AND DISCUSSION

3.1 Micro-TPV generator

We employ a realistic model of the μTPV system shown in Fig. 1 to calculate its overall efficiency. In this model, we include several sources of loss unique to a portable power-generation system: namely, the heating of the input gases (propane and oxygen) and lack of thermal recovery of hot exhaust gases, as well as emission off to the sides due to the finite thickness of our emitter (it is shaped like a box with dimension of 10 $\times$ 10 $\times$ 1.3 mm). We also assume that packaging considerations prevent the emitter and TPV diode from coming closer than 1.1 mm, which corresponds to a view factor of 80%. We also model our TPV diodes to have the same electrical characteristics found in Ref. [24]. Finally, we assume that due to the thermal tolerances of the experimental device, our temperatures cannot exceed 1100 K.

In the base case, we use a graybody emitter with flat emissivity, i.e., a silicon wafer. We find the maximum output at a flow rate of 12 sccm propane (corresponding to an input thermal flow of 18 W) is 340 mW, for an efficiency of 1.89%. If we then optimize a 1D PhC consisting of alternating layers of silicon and silicon dioxide, we find that the optimal structure has 3 bilayers with a period of 803 nm and a first layer of 434 nm. At an input flow rate of 9.58 sccm (14.36 W), the maximum output possible is 448 mW, for an efficiency of 3.12% – a 65% improvement.

Since both structures examined above experience substantial losses of photons emitted on the sides, we also examined what happens if platinum is put on the sides instead. We found that at an input flow rate of 7.70 sccm (11.55 W), the maximum output possible is 452 mW, for an efficiency of 3.91%. Furthermore, if platinum is used to coat the entire structure, and a thin layer of silica (429 nm) is placed on the faces pointed toward the TPV diodes, the maximum output is 184 mW at a flow rate of only 2.44 sccm (3.66 W), for an efficiency of 5.02%.

We also consider an emitter structure made entirely of tungsten, with a 2D array of holes etched into the faces pointed toward the TPV diode to enhance short-wave emissivity. We find in this case that the maximum output is 315 mW at a flow rate of 2.85 sccm (4.27 W) for an efficiency of 7.38%.

The overall performance of each design as a function of flow rate is summarized by Fig. 4.

If several of the input parameters were to be improved to their theoretical maximum values, namely temperature, view factor, and external quantum efficiency, then the overall device efficiency for the optimized 2D tungsten PhC structure could reach as high as 20.48%.

3.2 Solar TPV

A solar TPV system is a variant of TPV in which optical concentrators are used to collect heat from the sun, as shown in Fig. 2 [6, 10, 25–27]. The most important and unique attribute of solar TPV is its use of selective solar absorbers. The key figure of merit for the selective absorber is the maximum fraction of incident sunlight that can be captured as heat for a particular solar concentration C and equilibrium temperature T. The expression

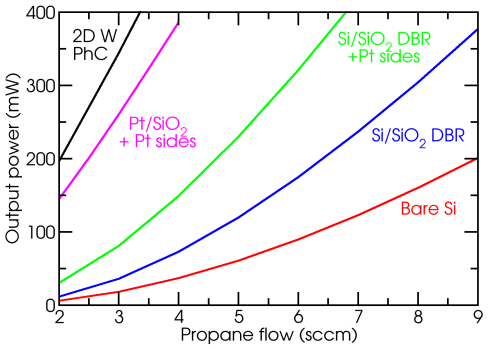

FIG. 4: Predicted output power for several selective μTPV selective emitters as a function of propane flow rate.

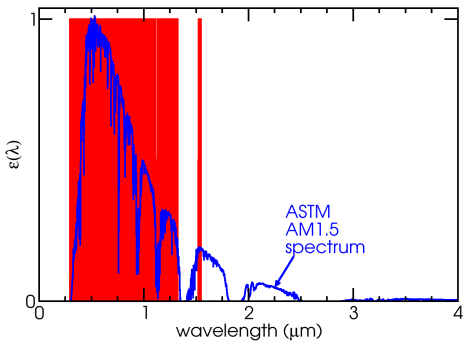

FIG. 5: The emissivity spectrum of an isotropic ideal selective solar absorber for $C = 2000$ and $T = 2120$ K, superimposed on the AM1.5 solar spectrum. Note the dips in both spectra at wavelengths around 1.3 μm, where atmospheric gases strongly absorb most incoming sunlight.

is given by [28]:

$$\eta_t = B\overline{\alpha} - \frac{\overline{\epsilon}\sigma T^4}{CI} \tag{8}$$

where I is the solar constant, σ is the Stefan-Boltzmann constant, B is the transmittance of the glass vacuum enclosure (taken in this manuscript to be 1), $\overline{\alpha}$ is the average absorbance, given by:

$$\overline{\alpha} = \frac{1}{I}\int_0^\infty d\lambda \int_0^{\theta_c} d\theta \left[\epsilon(\lambda,\theta)\sin 2\theta \frac{dI}{d\lambda}\right] \tag{9}$$

where $dI/d\lambda$ is the AM1.5 solar spectrum [29], and $\overline{\epsilon}$ is the angular-averaged emittance, given by:

$$\overline{\epsilon} = \frac{1}{\sigma T^4}\int_0^\infty d\lambda \int_0^{\pi/2} d\theta \left\{\frac{2hc^2\epsilon(\lambda,\theta)\sin 2\theta}{\lambda^5\left[e^{hc/\lambda kT}-1\right]}\right\}. \tag{10}$$

The angularly-dependent expression $\epsilon(\lambda,\theta)$ occurs in both $\overline{\alpha}$ and $\overline{\epsilon}$ because of Kirchoff's law; however, the first integration is only up to $\theta = \theta_c$, which increases with higher solar concentrations, due to geometric optics. In the remainder of this paper, we focus on the case of any absorber with maximum concentration in the polar direction, like the parabolic trough illustrated in Fig. 2, where $\theta_c = \pi/2$, or an isotropic emitter under any concentration. In this case, maximizing η_t is a conceptually straightforward exercise, wherein one sets emissivity to one for wavelengths where input sun power outweighs the thermally emitted power, and zero otherwise. An example of the ideal emitter spectrum for the particular situation of a concentration of 2000 suns and a temperature of 2120 K is shown in Fig. 5. Note that atmospheric absorption introduces distinct dips in what would otherwise be a simple step function. The overall thermal transfer efficiency of an optimized step function emissivity under these conditions is 68.8%.

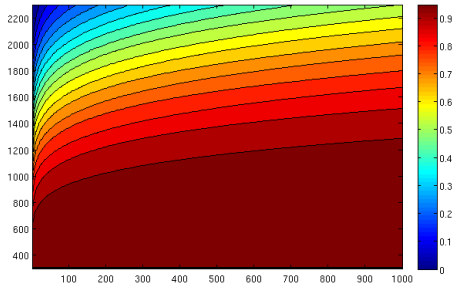

FIG. 6: The thermal transfer efficiency of ideal selective absorbers described in the text, as a function of solar concentration (x-axis) and temperature in K (y-axis).

However, using the tailored approach illustrated in Fig. 5 leads to an efficiency of 73.5% – a relative improvement of 6.8%.

The overall thermal transfer efficiency for a range of concentrations and temperatures has been calculated and illustrated in Fig. 6. As one might expect, thermal transfer is most efficient at high concentration and low temperatures, where the relative impact of radiation is lowest.

The maximum theoretical power conversion efficiencies for a single-junction TPV diode with bandgap E_g and a selective emitter with a top-hat emissivity function (equal to one for energies E_g to $E_g + \Delta E$ and zero otherwise) are displayed in Fig. 7. In order to introduce a degree of realism, reflectivities are assumed to be no greater than 99.9% for any wavelength. This prevents unreasonable results, such as extremely high efficiencies with large bandgaps at modest temperatures. As

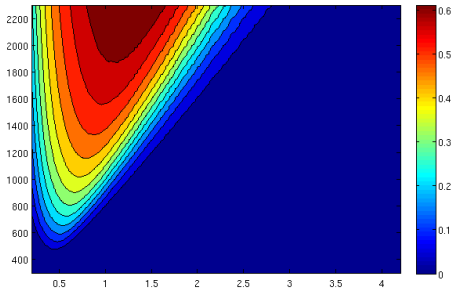

FIG. 7: Maximum efficiency of a TPV diode with bandgap E_g illuminated by a selective emitter of 100% emissivity for photon energies between E_g and $E_g + \Delta E$ only, and 0.1% emissivity otherwise, as a function of E_g (x-axis) and temperature (y-axis).

expected, higher temperatures allow for higher efficiencies, since they are bounded from above by the Carnot efficiency. Also, higher temperatures imply higher ideal bandgaps, in a nearly linear relationship.

Combining the results of Figs. 6 and 7, it is found that the maximum combined efficiencies of the ideal selective absorber and selective emitter system applicable to solar TPV, assuming a maximum concentration of 2000 suns (well below the theoretical maximum of 46200 suns) is 44.8% at a temperature of 2120 K, with a bandgap of 1.1 eV – close to that of crystalline silicon. This substantially exceeds the Shockley-Quiesser efficiency limit [30] for a single junction photovoltaic cell of 38% at 2000 suns [31].

4 CONCLUSION

In summary, we have presented a unique approach to modeling TPV systems that accounts for angular-sensitive emission – particularly important for surfaces with complex wavelength scale designs such as PhCs. We have used this approach to show that portable TPV systems, such as the μTPV laboratory system, can see up to a factor of 11 improvement in their efficiencies compared to a graybody emitter. We also demonstrated that solar TPV systems can be designed in two stages: first, by optimizing the thermal transfer efficiency of the selective absorber by maximizing the contribution for each wavelength separately, and second, by optimizing the range of selective emitter emission and the bandgap of the TPV diode. Even if the concentration is constrained to a maximum of 2000 suns, it is found that a single-junction TPV system at a temperature of 2120 K and with a bandgap of 1.1 eV can in principle offer an efficiency as high as 44.8%, thus exceeding the Shockley-Quiesser efficiency limit for a single junction photovoltaic cell at the same concentration.

[1] H. H. Kolm, Solar-battery power source, 1956, Quarterly Progress Report, Group 35, page 13.

[2] B. Wedlock, Proc. IEEE **51**, 694 (1963).

[3] R. Black, P. Baldasaro, and G. Charache, Thermophotovoltaics - development status and parametric considerations for power applications, in *International Conference on Thermoelectrics*, volume 18, pp. 639–644, 1999.

[4] J. Fleming, S. Lin, I. El-Kady, R. Biswas, and K. Ho, Nature **417**, 52 (2002).

[5] F. O'Sullivan, I. Celanovic, N. Jovanovic, J. Kassakian, S. Akiyama, and K. Wada, J. Appl. Phys. **97**, 033529 (2005).

[6] N. Harder and P. Wurfel, Semicond. Sci. Technol. **18**, S151 (2003).

[7] H. Xue, W. Yang, S. Chou, C. Shu, and Z. Li, Nanoscale Microscale Thermophys. Eng. **9**, 85 (2005).

[8] P. Bermel, M. Ghebrebrhan, W. Chan, Y. X. Yeng, M. Araghchini, R. Hamam, C. H. Marton, K. F. Jensen, M. Soljacic, J. D. Joannopoulos, S. G. Johnson, and I. Celanovic, Opt. Express (2010), accepted.

[9] W. Durisch, B. Bitnar, F. von Roth, and G. Palfinger, Solar Energy **75**, 11 (2003).

[10] A. Datas, C. Algora, V. Corregidor, D. Martin, A. Bett, F. Dimroth, and J. Fernandez, AIP Conf. Proc. **890**, 227 (2007).

[11] J. D. Joannopoulos, S. G. Johnson, J. N. Winn, and R. D. Meade, *Photonic Crystals: Molding the Flow of Light*, 2nd ed. (Princeton, Princeton, NJ, 2008).

[12] U. Ortabasi and B. Bovard, AIP Conf. Proc. **653**, 249 (2003).

[13] T. D. Rahmlow, D. M. DePoy, P. M. Fourspring, H. Ehsani, J. E. Lazo-Wasem, and E. J. Gratrix, AIP Conf. Proc. **890**, 59 (2007).

[14] J. M. Gee, J. B. Moreno, S.-Y. Lin, and J. G. Fleming, Selective emitters using photonic crystals for thermophotovoltaic energy conversion, in *Twenty-ninth IEEE Photovolt. Spec. Conf.*, 2002.

[15] A. Heinzel, V. Boerner, A. Gombert, B. Blasi, V. Wittwer, and J. Luther, J. Mod. Opt. **47** (2000).

[16] H. Sai, Y. Kanamori, and H. Yugami, Appl. Phys. Lett. **82**, 1685 (2003).

[17] M. Ghebrebrhan, Y.-X. Yeng, P. Bermel, I. Celanovic, M. Soljacic, and J. D. Joannopoulos, Tailoring thermal emission via q-matching of photonic crystal resonances, Submitted to Phys. Rev. A.

[18] E. Eckert and E. Sparrow, Int. J. Heat Mass

Transfer **3**, 42 (1961).
[19] S. Sze, *Physics of Semiconductor Devices* (Wiley and Sons, New York, 1981).
[20] P. Bienstman, *Rigorous and efficient modelling of wavelength scale photonic components*, PhD thesis, University of Ghent, Belgium, 2001.
[21] D. Delbeke, *Design and fabrication of a highly efficient light-emitting diode: the grating-assisted resonant-cavity light-emitting diode*, PhD thesis, University of Ghent, Belgium, 2002.
[22] P. Bermel, C. Luo, L. Zeng, L. Kimerling, and J. D. Joannopoulos, Opt. Express **15**, 16986 (2007).
[23] M. Ghebrebrhan, P. Bermel, Y. Avniel, J. D. Joannopoulos, and S. G. Johnson, Opt. Express **17**, 7505 (2009).
[24] W. Chan, R. Huang, C. A. Wang, J. Kassakian, J. D. Joannopoulos, and I. Celanovic, Sol. Energy Mater. Sol. Cells **94**, 509 (2010).
[25] W. Spirkl and H. Ries, J. Appl. Phys. **57**, 4409 (1985).
[26] A. Luque, AIP Conf. Proc. **890**, 3 (2007).
[27] E. Rephaeli and S. Fan, Opt. Express **17**, 15145 (2009).
[28] Q.-C. Zhang, J. Phys. D: Appl. Phys. **32**, 1938 (1999).
[29] ASTMG173-03, *Standard Tables for Reference Solar Spectral Irradiances: Direct Normal and Hemispherical on 37 degree Tilted Surface* (ASTM International, West Conshohocken, Pennsylvania, 2005).
[30] W. Shockley and H. J. Queisser, J. Appl. Phys. **32**, 510 (1961).
[31] C. Henry, J. Appl. Phys. **51**, 4494 (1980).